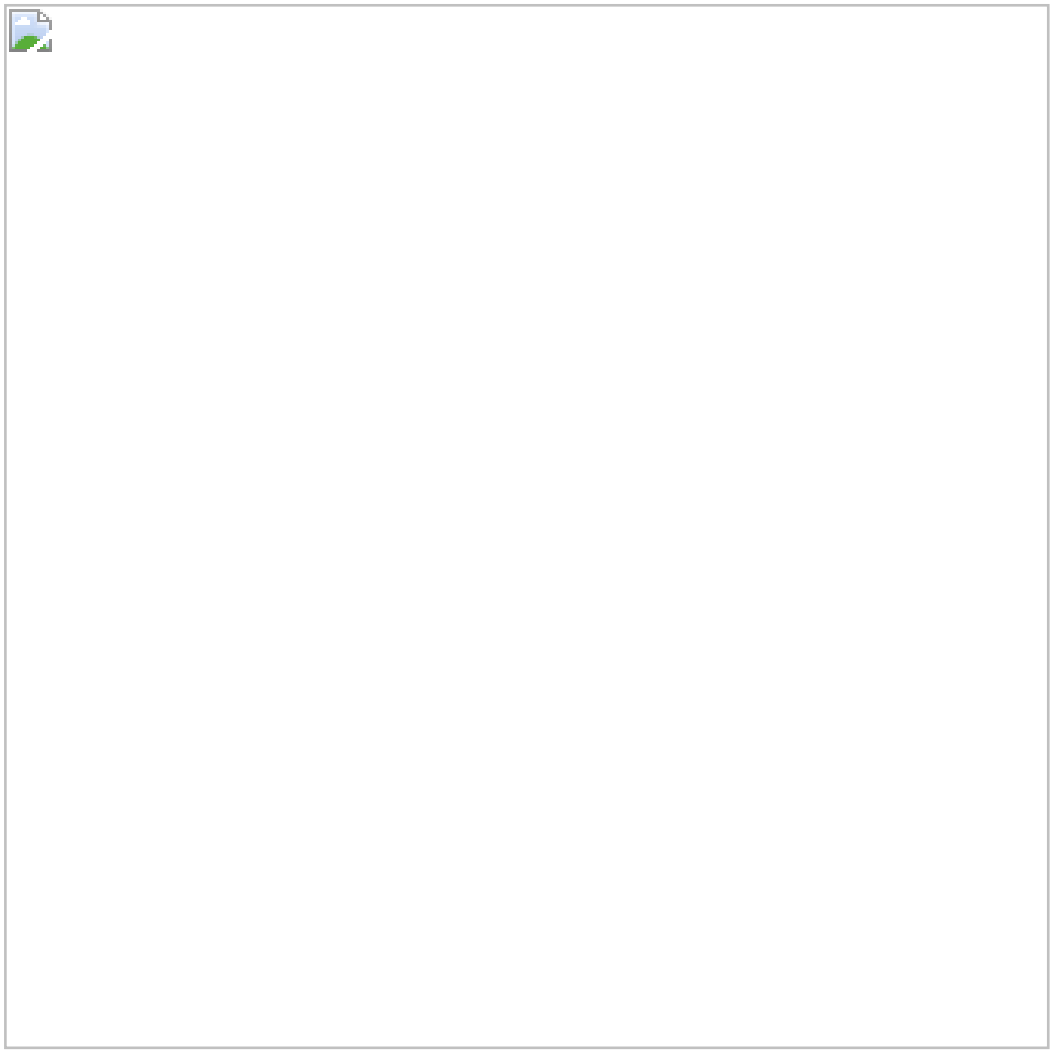

Land Use/Cover Changes and Surface Temperature Dynamics Over Abaminus Watershed, Northwest Ethiopia

Authors: Debie, Ermias, Anteneh, Mesfin, and Asmare, Tadele

Source: Air, Soil and Water Research, 15(1)

Published By: SAGE Publishing

URL: https://doi.org/10.1177/11786221221097917

Land Use/Cover Changes and Surface Temperature Dynamics Over Abaminus Watershed, Northwest Ethiopia

Air, Soil and Water Research
Volume 15: 1–16

DOI: 10.1177/11786221221097917
SAGE

Ermias Debie[1], Mesfin Anteneh[1] and Tadele Asmare[2]

[1]Bahir Dar University, Ethiopia, and [2]Debre Markos University, Ethiopia

ABSTRACT: The study investigates the impact of land use/cover changes on the dynamics of surface temperature in the Abaminus watershed, Northwest Ethiopia. Landsat-5 images of 1987, 1999, and 2010, and the Landsat-8 image of 2018 were used as the sources of data. The land use/cover changes were calculated using a land-use transition matrix. Data generated from household surveys were presented using percentage values to identify the driving forces of land use/cover changes. The land surface temperature (LST) result was quantified using the respective index equation. Results indicated that wetland, forest, shrublands, and grasslands declined by 96.6%, 72%, 77.7%, and 89.4% respectively over the analysis period. The encroachment of cultivation and overgrazing to marginal lands, weak institutional arrangement, sedimentation, high drainage of wetlands for crop production, and recurrent drought were the major driving forces behind the land use/cover change. Within this effect, the average land surface temperature was increased by 11.5°C, 3.22°C, and 2.02°C due to wetland loss, clearing of the forest, and decline of shrublands respectively for the last 31 years. LSTs had correspondingly decreased by 5.42°C and 3.77°C on the afforested barren surfaces and planted shrublands. Hence, there should be an improved institutional arrangement for managing open access resources through the participation of local people in the management for minimizing the increase of land surface temperature in the study watershed. Moreover, enclosure management and plantation of multipurpose species on degraded communal lands shall be scaled-up to significantly reduce land surface temperatures.

KEYWORDS: Land use/cover dynamics, surface temperature, Abaminus mountain, northwest Ethiopia

TYPE: Original Research

CORRESPONDING AUTHOR: Mesfin Anteneh, Department of Geography and Environmental Studies, Bahir Dar University, Bahir Dar, Ethiopia. Email: mesfin74@yahoo.com

Background

Land use/cover is the interface between the atmosphere and the biosphere for material and energy exchange. Land use/cover changes (LUCCs) are triggered by the interplay of socio-economic and natural environmental factors. Inappropriate farming practices, overgrazing, rapid growth in the human population (Assefa & Singh, 2017; Dinka & Chaka, 2019; Liyehu et al., 2019; Twisa & Buchroithner, 2019; Ullah et al., 2019), and weak institutional setup (Dinka & Chaka, 2019) are among the key anthropogenic driving variables of LUCCs. Climate change (Kleemann et al., 2017; Ullah et al., 2019) is the significant natural factor triggering LUCCs. Climate variability influences the succession of plant and animal species over fragile mountain ecosystems. Rapid changes in the human population initiate the encroachment of farming and grazing to the fragile surface topography. Advances in technology and weak institutional response promote uncontrolled lumber cutting and overuse of communal mountain resources that further encourage increased land degradation and LUCCs.

The LUCCs pose multi-dimensional impacts on local climatic and environmental systems. The event influences the temporal and spatial dynamics of environmental and ecological systems including greenhouse gas emissions (Pandey et al., 2017); biodiversity losses (Barlow et al., 2016; Ellis et al., 2012); soil erosion and sedimentation (Assefa & Singh, 2017; Birhanu et al., 2019; Butt et al., 2015; Debie et al., 2019; Dinka & Chaka, 2019; Gessesse & Bewket, 2014; Liyehu et al., 2019); hydrologic processes (Birhanu et al., 2019; Butt et al., 2015; Dinka & Chaka, 2019); and climate change (Brovkin et al., 2013). This further results in the decline of crop production and forage shortages for feeding livestock (Assefa & Singh, 2017; Debie et al., 2019; Dinka & Chaka, 2019; Gessesse & Bewket, 2014).

Change in Land use/cover (LUC) directly causes changes in the physical characteristics of the land surface, which affects radiation, heat, and water vapor exchange. LUCCs influence surface energy balance, which is the major underlying process for temperature change (Jain et al., 2017), and other extreme weather events like droughts and flooding (Pandey et al., 2017; Ullah et al., 2019). For instance, anthropogenic and LUCC induced warming has been accounting for a quarter of the overall temperature rise since the year 2001 (Gogoi et al., 2019). The gain of no vegetation classes, such as built-up landscape, barren surface, and croplands to the loss of vegetation covers and wetlands caused the rise of the highest mean land surface temperature (Balew & Korme, 2020; Gogoi et al., 2019; Haylemariyam, 2018; Mushore et al., 2017; Zhou & Wang, 2011). The vegetation and surface water bodies' degradation affects the absorption of solar radiation, surface temperature, evaporation rates, storage of heat, wind turbulence, and can change the near-surface atmosphere conditions. Whilst, water body, and vegetation cover played an important role in mitigating the land surface temperature effect (Zhou & Wang, 2011).

In Ethiopia, the dynamics of LUC accompanied by surface temperature variability became a common phenomenon since the 20th century (Hurni et al., 2010). Land surface temperature (LST) is the skin temperature of the surface which refers to soil surface temperature for bare soil and canopy surface temperature for vegetation cover with varied characteristics of the land (Pal & Ziaul, 2017). It is a reflection of the energy flow in the interactions between the land surface and atmosphere/biosphere. The LST is determined by the effective radiating temperature of the land's surface that controls through the process of surface energy and water exchange with the atmosphere (Yuan & Bauer, 2007; Zhang & He, 2013). It uses to extract information from various features of the land surface (Sinha et al., 2015).

The impacts of LUCCs on environmental recession can be measured by land surface temperature (LST) differences in diverse attributes of the landscape (Zhang et al., 2016). Significant LST differences can exist over the different LUC units and changes because each land cover type possesses unique qualities of radiation and absorption (Ahmed et al., 2013; Lai et al., 2012; Sinha et al., 2015). As the LUC pattern is getting changed, its imprint is reflected on LST (Pal & Ziaul, 2017). Surface temperature variation can be identified when one type of land cover is converted to another. A range of studies in South East Asia indicated that the types and charters of land cover significantly affect LST variation and distribution. For instance, the proportion of vegetation covers and water bodies per grid cell has a negative significant correlation with LST variance (Lai et al., 2012; Li et al., 2013; Peng et al., 2017; Wenga et al., 2004; Xiao et al., 2008). Alternatively, the percentage of built-up and impervious land or barren surface areas have a positive correlation with LST dynamics (Lai et al., 2012; Xiao et al., 2008). Although the accelerated rate of wetlands and vegetation degradation observed in the upper Blue Nile basin northwest Ethiopia (Birhanu et al., 2019; Hurni et al., 2010), studies linking LUC units and changes to land surface temperature changes are few, they are limited to vegetation cover (Meseret, 2019), and urbanization related aspects (Balew & Korme, 2020; Haylemariyam, 2018).

LST is an important parameter for environmental studies of earth surface and terrestrial radiation over large spatial and temporal scales for agro-meteorology monitoring (Zhang & He, 2013). The change in LST is a regional climate response to global climate change and has research significance in agriculture, hydrology, ecology, environment, climate, and biogeochemistry (He et al., 2017). A study on the relationship between LST and LUCCs is essential to address regional environmental problems and provide a basis for regional planning. Retrieving LST from satellite data at regional and local scales has an advantage of a wide observation range and strong spatial continuity, in particular in areas where meteorological data are difficult to obtain. It provides new evidence to fill the knowledge gap in the local-scale temperature effects of different landscape characters and biophysical changes induced by anthropogenic activity. Thus, the focus of this study is mainly aimed to assess the change that occurred in LUCs of the Abaminus watershed from 1987 to 2018, and establish its association with LST dynamics in the upper Blue Nile Basin of Northwest Ethiopia. The findings of this study were proposed pertinent mechanisms for sustainable use of land resources and then decreasing of surface temperature distribution on barren and no vegetation areas.

Materials and Methods

Description of the study area

The Abaminus watershed is part of the upper Blue Nile Basin in the northwest highlands of Ethiopia. The watershed lies between 10°38′6.161″N and 11°8′48.328″N latitude and 38°5′12.436″E and 38°31′49.06″E longitude.

The total area of the study watershed covers about 172,142.2 ha, and it is characterized by diverse topographic conditions. Gently sloping to slightly undulating plains, rugged and dissected hilly mountains and relatively deep river gorges characterize the entire relief. The local climate is dominantly humid sub-tropical. The watershed in general falls within three agro-climatic zones (cool-moist, tepid-moist, and warm highlands) that are equivalent to the Ethiopian traditional agro-ecological zones of *Dega*, *Woina-Dega*, and *Kola*, respectively with the elevation ranges from 1,145 to 3,534 m.a.s.l. (Figure 1). Rainfall varies spatially from 1,326.5 mm over the cool-moist agroecology to 917.9 mm in the warm highlands agroecology. More than three-fourths of the total rainfall occurs during the summer season (from June to September).

In all agro-ecological zones of the watershed, subsistence primitive crop-livestock mixed-farming agriculture is the predominant livelihood activity. Conventional tilling through a hand press with ox-pulling traditional technique is the most common one of all crop productions. In the *Dega* agro-ecological zone (⩾2,800 masl cool-moist highlands) barley (*Hordeum vulgare*) and potato (*Solanum tuberosum*) are chiefly produced. Degradation and soil acidity are most likely serious problems over the steeper hill slopes in this agroecology. In the *Woina-Dega* agro-ecological zone, tef (*Eragrostis tef*), barley (*Hordeum vulgare*), wheat (*Triticum vulgare*), and horse beans (*Vicia faba*) are common crops. Tef (*Eragrostis tef*) and Wheat (*Triticum vulgare*) are predominantly grown crops among the others. In the *Kola* agro-ecological zone, sorghum is largely produced. Crop production in the agro-ecological zone is suffering perhaps due to erratic rainfall and severe ecological degradation.

Communal and privately owned lands and livestock are the most important livelihood assets of the local community in all of the agroecological zones. The common-pool resources (forests, shrublands, wetlands, and grasslands) are usually managed by the local community and administration units. The hilly and

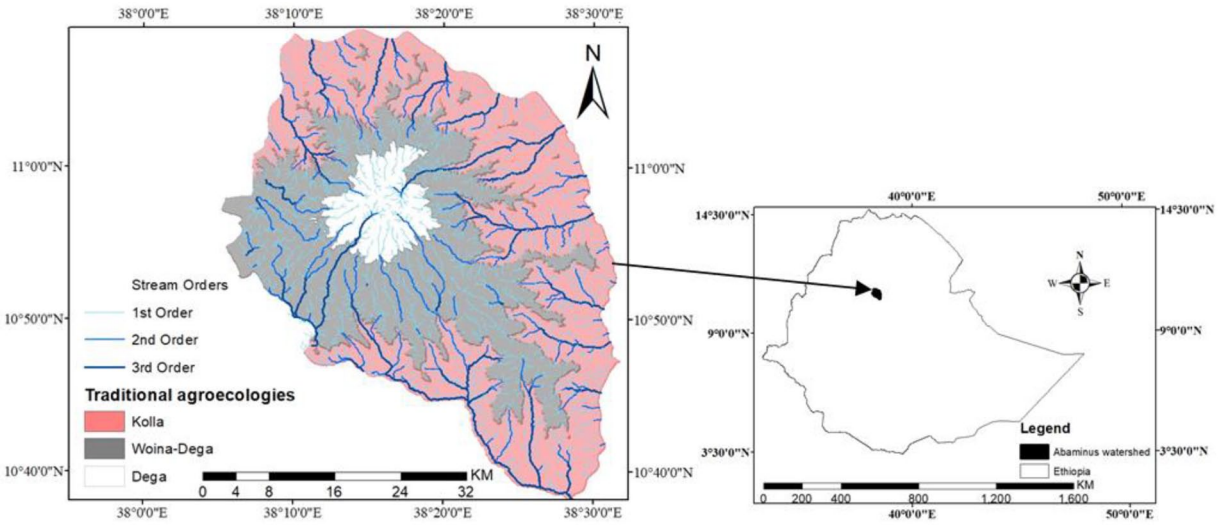

Figure 1. Map of the study watershed.

Table 1. Descriptions of Land Use/Cover Classes.

CLASS/USES	DESCRIPTIONS
Wetlands	All forms of water, including rivers, lakes, ponds, and swamps
Forests	Natural and afforested distributed vegetation with dense canopies
Shrublands	Natural and man-made vegetation dominated by shrubs, including grasses, herbs, and bushes
Grasslands	The mixtures of grasslands and other forms of undergrowth
No vegetation	Including harvested cropland, barren surfaces (soil, roads sandy, and rocky), and settlement

steep slope communal lands of the watershed are highly threatened by vegetation degradation and dissected by gullies due to uncontrolled overgrazing.

Cattle, sheep, goat, donkey, and horse are reared under the cut-and-carry and open-grazing systems. Local labor and firewood/charcoal/sales are alternative means of farmers' livelihoods to meet household food demands, particularly in kola agroecology.

In the study watershed, five major LULC classifications, such as forests, shrublands, grasslands, no vegetation, and wetlands are identified (Table 1). Privately owned individual farmer-managed settlements and croplands are the largest land-use systems in the area.

Methodology

Data sources and collection techniques

Remote sensing data are important primarily to understand the degree of interaction between the social and ecological systems. Space-based observations of Landsat TM (Thematic Mapper) image of 1987, 1999, and 2010, and Landsat-8 Operational Land Imager (OLI) image of 2018 were acquired from the US Geological Survey (USGS; http://glovis.usgs.gov/). Clear-sky and similarity of the ambient temperature were considered for the selection of 4-year satellite imagery data. For each year, cloud-free from January to February, and one frame with Path 169 and Row-052 satellite imagery data were acquired. The Landsat TM and OLI are usually capable of mapping vegetation, moisture, water bodies, and LST dynamics analysis at the watershed level (Bai et al., 2008). Based on the results of LUCCs detection, three *Kebeles* (small administrative units) were purposely selected across three traditional agro-ecologies. The high rate of conversion from vegetation and wetland into no-vegetation was the main criterion to select *Geses* from *Kola*, *Yebuchir-Yewoya* from *Woina-Dega*, and *Dequat-Goshera* from *Dega* agroecology. From the selected *Kebeles*, about 164 household heads were selected using a systematic sampling technique. A household survey was conducted with the selected household heads using a semi-structured questionnaire.

Methods and Procedures of Analysis

Calculation of spectral indices

When the land surface reflectance is measured, an atmospheric correction should perform to correct for atmospheric effects on satellite scenes (Zhang et al., 2010).

Table 2. Bands Micrometers and Resolution of Thematic Mapper (Landsat-5) and Operational Land Imager (Landsat-8).

LANDSAT	BANDS		WAVELENGTH (MM)	RESOLUTION (M)
Landsat-5™	Band 2	Green	0.52–0.60	30
	Band 3	Red	0.63–0.69	30
	Band 4	NIR (near-infrared)	0.77–0.90	30
	Band 5	MIR (middle infrared)	1.55–1.74	30
	Band 7	MIR (middle infrared)	2.9–2.35	30
	Band 6	Thermal infrared	10.40–12.50	60 × 30
Landsat-8 OLI	Band 3	Green	0.53–0.59	30
	Band 4	Red	0.64–0.67	30
	Band 5	NIR (near-infrared)	0.85–0.88	30
	Band 6	MIR (middle infrared)	1.57–1.65	30
	Band 7	MIR (middle infrared)	2.11–2.29	30
	Band 10	Thermal infrared (TIR)1	10.6–11.19	100
	Band 11	Thermal infrared (TIR)2	10.50–12.51	100

The spectral indices' raster of six bands of Landsat-5 and 8 with a 30 m spatial resolution was used to classify the land use/covers and to quantify LST (Table 2). Spectral indices are the combinations of spectral reflectance from two or more wavelengths that indicate the domination of certain characteristics of land cover (Gašparović et al., 2019). Normalized difference vegetation index (NDVI), modified normalized difference water index (MNDWI), normalized difference soil index (NDSI), and normalized difference bareness index (NDBaI) were applied to develop spectral indices.

The main principle of detecting vegetation using NDVI is vegetation highly reflective in the near-infrared and high absorptive vegetation pigments (chlorophyll) in the visible red. The contrast between these channels can be used as an indicator of the status of the vegetation.

$$\text{NDVI can be computed as } \frac{\text{Near infrared} - \text{Visible red}}{\text{near infrared} + \text{Visible red}} \quad (1)$$

Where Near-infrared represents band 4 in Landsat-5 and band-5 in Landsat-8. Red represents band-3 for Landsat-5 and band-4 for Landsat-8.

The NDVI is a biophysical parameter that relates to photosynthetic vegetation to offer valuable information about the dynamics of vegetation covers over time (Xie et al., 2008). From other various available vegetation indices, the NDVI is widely employed since it normalizes the effect of changes in illumination conditions and surface topography (Reddy & JangaReddy, 2013). Genesis et al. (2015) recommend that a linear model with NDVI time-series analysis, perhaps use to best fit the cyclic vegetation difference into a line. Values of NDVI ranges from −1 to 1, where vegetated areas generally result in high values because of their relatively high near-infrared reflectance and low visible reflectances. Determination of the threshold value is the main problem of the automatic extraction of individual land cover classification from a single index raster. It is a difficult and lengthy process (Xian et al., 2009). Value ranges of the index for different land cover/use types can be found in certain ranges and are specific to each satellite imagery scene (Lee et al., 2011). The K-means unsupervised classification method can be used to extract a specific single index raster (Li et. al, 2017). It was used as a popular algorithm for classifying NDVI data into k-clusters, such as grasslands, shrublands, and forests. Vegetation class was classified into sparse for grasslands, moderate for shrublands, and dense to forests.

Modified normalized difference water index (MNDWI) is one of the methods of remote sensing to measure surface water characteristics where field investigations are difficult to carry out (Soti et al., 2009). It is mostly computed by using (Xu, 2006):

$$\text{MNDWI} = \frac{\text{GREEN} - \text{MIR}}{\text{GREEN} + \text{MIR}} \quad (2)$$

The indices of MNDWI range between 1 and −1. This requires reclassification to classify surface water from other land use land covers. Indices greater than zero, commonly represent standard thresholds to detect the distribution and extent of surface water (Xu, 2006). The MNDWI is one the most widely used water indices for surface water mapping as the built-up land, soil, and vegetation all have negative values and thus is notably suppressed and even removed (Campos et al., 2012;

Duan & Bastiaanssen, 2013; Hadeel et al., 2011; Poulin et al., 2010).

The combination of the normalized difference bareness index (NDBaI) with the normalized difference soil index (NDSI) is the proper method to derive the accuracy class of no vegetation (Zhao & Chen, 2005).

$$NDSI = \frac{MIR - Green}{MIR + Green} \quad (3)$$

Where, MIR is band-5 for the reflectance of Landsat-5 and band-7 for Landsat-8 and the Green represents band-2 for Landsat-5 and band-3 for Landsat-8 (Deng et al., 2015). This is attributable to only soil more reflective in band-5 of Landsat-5 and band-7 of Landsat-8 (Rogers & Kearney, 2004).

Normalized difference bareness index (NDBaI) was proposed to recognize different types of bare areas that formed due to physiographic and anthropogenic factors (Li et al., 2017; Zhao & Chen, 2005). The index is based on significant differences in the spectral signature in the near-infrared between bare soil and background. The NDBaI is calculated as follows (Zhao & Chen, 2005):

$$NDBaI = \frac{SWIR1 - TIR}{SWIR1 + TIR} \quad (4)$$

Where, SWIR1 is a short-wavelength infrared band, such as Landsat-5 band-5 and Landsat-8 band-6 and TIR is the thermal infrared band, such as band-6 for Landsat-5 and band-10 for Landsat-8. Based on the k-mean unsupervised classification, the class with the highest mean value represents bare land and the second class represents the built-up class (Li et al., 2017).

All spectral indices were calculated using the raster based on the respective index equation. The maximum likelihood supervised classification was used to compare the results K-means unsupervised method. It calculates the relative class membership likelihoods incorporating all training sets for each pixel in an image. All rasters with an extracted certain land cover were merged to generate land use and cover classes in one raster. According to the mean value of the classified indices, the automatic algorithm extracts the final land cover classes. The LUCCs were calculated using a land-use transition matrix. It indicates the amount of different land uses/covers that remain unchanged and quantifies the gains and losses during the study periods. The method is employed to describe the conversion size land-use types in three periods. The matrices of land-use transition were developed in the first period from 1987 to 1999, the second period from 1999 to 2010, and the third period from 2010 to 2018. Factors that drive the conversion of one LUC into another LUC were described in percentage (Figure 2).

LST extraction from thermal bands

Developing methodologies to measure land surface temperature (LST) from space is being increasingly recognized (Li et al., 2013). The use of satellites in the TIR is important to estimate reliable LST over large spatial and temporal scales as it is practically difficult to obtain such information from ground-based measurements (Ermida et al., 2017). LST is detected by infrared thermal sensors and provides finer spatial resolution only under clear-sky conditions (Liang et al., 2019). The atmospheric effects on top of atmosphere (TOA) spectral radiance are usually administered by atmospheric transmittance (T), atmospheric path radiance (*Lu*), and sky radiance (*Ld*) (Chatterjee et al., 2017). The spectral radiance model was employed to retrieve LST from Landsat-5 TM and Landsat-8 OLI (Hua & Ping, 2018). Thermal infrared data (band-6 from Landsat-5 and band-10 from Landsat-8) were used. From Landsat-8, thermal band-10 was used because thermal band-11 data are significantly more contaminated by thermal energy from outside the thermal field of view (stray light) than band 10 (USGS, 2016). The thermal infrared bands were used to estimate LSTs according to the reference values, calibration data, and empirical models widely used in land surface climate studies.

Conversion of digital number into spectral radiance. Based on the reference values in the sensor handbook, the digital number (DN) values convert into spectral radiance ($L\lambda$) (USGS, 2016). The conversion of DN values of the thermal bands into absolute radiance values is the standard method for retrieving LST from the raw Landsat dataset (Chander et al., 2009; USGS, 2016; Weng, 2009). The DN is converted into space reaching radiance or top-of-atmospheric (TOA) radiance that is directly measured by remote sensing instruments (Chander & Markham, 2003). The TOA reflectance is a unitless measurement that provides the ratio of radiation reflected by the incident solar radiation on a given surface. It compensates for different values of solar irradiance arising from spectral band differences.

In Landsat-5, TOA or spectral radiance ($L\lambda$) was computed as:

$$L\lambda = \frac{\left(Lmax\lambda - Lmin\lambda\right)}{\left(Qcalmax - Qcalmin\right) x \left(Band\,6 - Qcalmin\right) + Lmin\lambda} \quad (5)$$

where; $L\lambda$ is TOA radiance at the sensor's aperture in watts/($m^2 \times ster \times \mu m$); $L_{max}\lambda$ is radiance maximum constant value from the metadata file of the band 6, $L_{min}\lambda$ is radiance minimum constant value from the metadata file of band 6, Q_{calmax} is the Quantize–Cal-Max constant values from the metadata file of band 6, and Q_{calmin} is Quantize–Cal-Min constant values from the metadata file of the band 6.

$$\text{In Landsat} - 8, \text{spectral radiance computed as } L\lambda = ML\lambda \times \text{Band10} + AL \quad (6)$$

where; $L\lambda$ represents the spectral radiance, ML represents the band-specific multiplicative rescaling factor, and AL represents the band-specific additive rescaling factor.

Conversion of spectral radiance (Lλ) to brightness temperature (T). After converting a digital number to reflection, the TOA radiance was then converted to the surface leaving radiance or brightness temperature by removing the effects of the atmosphere in the thermal region (Barsi et al., 2005). It is calculated with an assumption of unity emissivity and using pre-launch calibration constants. The following equation was used in the tool's algorithm to convert reflectance to brightness temperature (T).

$$T = \frac{K2}{\ln\left(\frac{K1}{L\lambda} + 1\right)} \quad (7)$$

Where T is the temperature in Kelvin (K), K1 is the pre-launch calibration constant 1 in W/(m² srμm), K2 is the pre-launch calibration constant 2 in Kelvin (K) and $L\lambda$ is spectral radiance. For obtaining the results in degree Celsius (°C), the radiant temperature is revised by adding the absolute zero (approximately −273.15°C), implying that $C = T - 273.15$.

The emissivity correction. The calculated radiant temperature was corrected for emissivity by using the NDVI values. After converting the brightness temperature values into degree Celsius (°C), the emissivity corrected LST was calculated as (Sobrino et al., 2004):

$$\text{Emissivity}(E) = 0.004 \times PV + 0.986 \quad (8)$$

$$\text{Where, the proportion of vegetation (PV)} = \left(\frac{[NDVI - NDVImin]}{[NDVImax - NDVImin]}\right)^2$$

The last step of the LST or emissivity-corrected LST was retrieved (Grover & Singh, 2015) as

$$LST = \frac{T}{1 + \left(\frac{\lambda T}{p}\right) \ln E\lambda} \quad (9)$$

Where, LST is the land surface temperature in Celsius, T is at sensor brightness temperature (°C) in equation seven, λ is The wavelength emitted radiance for which peak response and the average of limiting wavelength of band-10 or band-6 (Table 2), $E\lambda$ is the calculated emissivity value, and $p = h \times c/\alpha = 1.438 \times 10^{-2}$ mk, where α is the Boltzmann constant (1.38×10^{-23} JK^{-1}), h is Planck's constant (6.626×10^{-34} Js) and c is the velocity of light (3.0×108 ms^{-1}).

Statistical analysis

Descriptive statistics, such as percentage, range, and mean were used to analyze the changes of land use/covers and land surface temperature. Data generated from household surveys were presented using percentage values to identify the driving forces of land use/cover changes. The mean, range, and standard deviation of each LUCs and LST change were calculated using ArcGIS software. Simple linear regression was used to show the LST change over three decades. Data generated from household surveys were presented using percentage values to identify the driving forces of land use/cover changes.

Results and Discussion

Dynamics of land surface temperature (LST)

Figure 3 indicates land surface temperature (LST) distributions were varied from 4.99°C to 44.1°C in 1987, from 7.5°C to 45.93°C in 1999, from 9.5°C to 43.1°C in 2010, and from 10.1°C to 43.4°C in 2018. In all years, the high LST was distributed in the lower elevation of the study area (Figures 1 and 3). The influence of elevation also significantly affects LST (Peng et al., 2017). LST significantly raised with decreased altitude, implying that in the area with a relatively high elevation difference the LST noticeable vertical variation of decrease with altitude increase (Deng et al., 2018). This may be due to LST being affected by air temperature decrease with elevation and the surface vegetation in a high elevation area is relatively good. In high elevation areas, therefore, the solar radiation received by the ground surface mostly spread in the latent heat form and the LST is low.

The average LST was 27.9°C in 1987, 30.8°C in 1999, 30.83°C in 2010, and 31.65°C in 2018 (Figure 4). Results from curve fitting regression indicate that consistent increment of mean LST was explained by time at $R^2 = .824$ over three decades. The LST was increased by 2.88°C, 0.01°C, 0.79°C in the first period (from 1987 to 1999), in the second period, and the third period of the study in that order (Figure 5). In the first period, the highest LST change was observed when compared to other periods of the study. This may be due to the occurrence of metrological drought across the study area in 1999, which in turn contributes to the increment of LST on vegetation biomass. Over three decades, the mean LST was increased by 3.67°C. Based on the dataset from 1850 to 2015, the mean land surface air temperature has increased by 1.53°C, while global mean surface temperature has increased by 0.87°C (Jia et al., 2019). Inconsistent with the global warming trend, the mean LST was increased by 3.88°C in the last 20 years (Tan et al., 2020) and by 0.10°C year^{-1} (Zhao et al., 2019) in China. The land surface temperature of most of the areas of all land cover features have significantly increased overtimes (Majumder et al., 2020; Zhao et al., 2019). Land degradation due to land use/cover changes contributes to about 23% of anthropogenic emissions of carbon dioxide (CO_2), methane (CH_4), and nitrous oxide (N_2O) (Jia et al., 2019).

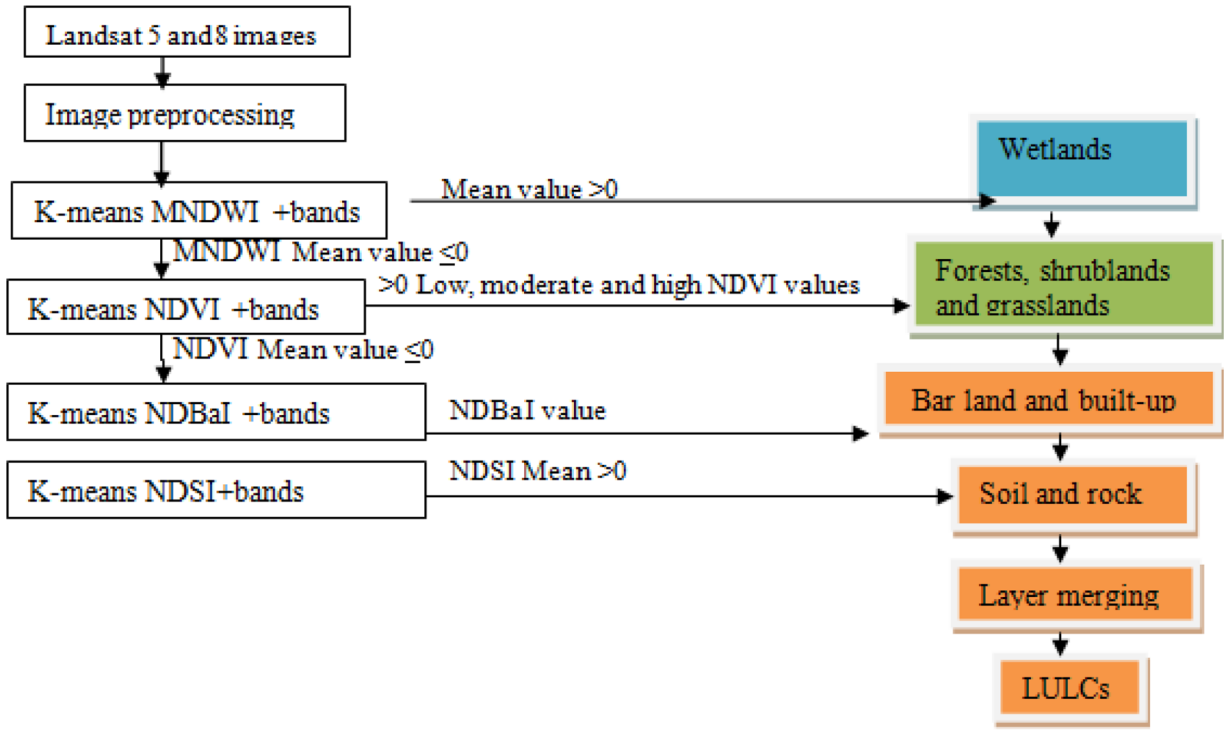

Figure 2. Workflow of LUCs analysis method.

Land use/covers (LUCs) and land surface temperature (LST) distribution

Of the total area, the forest cover was 8%, 7.2%, 4.5%, and 3.2% in 1987, 1999, 2010, and 2018, respectively (Figure 3). In the forest area, the average value of LST was 25.27°C over 31 years (Figure 4).

The forest cover declined by 8,220.5 ha over 31 years, implying that on an average 265.2 ha year^{-1} forest degradation (Figure 6). Deforestation was carried out on 1,386.1, 4,660.8, and 2,173.6 ha lands in the first period (from 1987 to 1999), in the second period (from 1999 to 2010), and the third period (from 2010 to 2018), in that order (Figure 6). This implies that on average, 115.51, 423.71, and 271.7 ha year^{-1} forest areas were cleared in the first, second, and third periods of the area, respectively. In the second period, deforestation was higher by 308.2 and 152.01 ha year^{-1} compared to the first and third periods, respectively. Concerning deforestation and other global factors, the average LST was varied from 23.75°C in 1987 to 26.54°C in 2018, implying that it was increased by 2.79°C over 31 years in the forest area (Figure 7).

From the total, shrubland contained 16.7% in 1987, 17.1% in 1999, 14.2% in 2010, and 9.6% in 2018. From 1987 to 2018, 12141.4 ha shrublands were lost, with an average of 391.66 ha year^{-1} (Figure 6). Over the three decades, the average LST was 28.2°C in the shrublands (Figure 7). Shrubland coverage was increased by 771 ha in the first period, while it was declined by 5,080.2 ha in the second period (Figure 6). In the third period, shrubland was decreased also by 7,832.2 ha. The average clearing rate of shrubland was increased by 517.2 ha year^{-1} in the third period compared to the second period. In the shrublands, LST was increasing from 26.57°C in 1987 to 28.98°C in 2018, indicating that it was increasing by 2.4°C over the 31 years (Figure 7).

The analysis of LUC dynamic trends over the 31 years showed grassland covered 12.5% in 1987, 10.4% in 1999, 8.4% in 2010, and 7.6% in 2018. The coverage proportion was consistently decreasing by 8,380.3 ha over the three decades, with an average of 270.33 ha year^{-1} (Figure 6). Grassland area decreased by 3,654.6, 3,485, and 1,240.7 ha in the first, second, and third periods in that order (Figures 6 and 8). This further implies that an average grassland area was decreasing by 304.55, 316.82, and 155.1 ha year^{-1} in the first, second, and third periods, respectively. During the second period, the mean lost grassland was higher by 12.27 and 161.72 ha year^{-1} when relatively seen for the first and third periods, respectively. In the grassland area, LST increased from 27.82°C in 1987 to 30.54°C in 2018, signifying that it was increasing by 2.72°C over the three decades (Figure 7).

Areas with no vegetation were covered by 61.7% in 1987, 64.9% in 1999, 72.7% in 2010, and 79.4% in 2018 (Figure 6). In the area with no vegetation, the mean LST was 32.3°C over the three decades (Figure 7). The highest average LST was retrieved from the area with no vegetation cover when compared to other LUCs (Figure 7). The average value of LST over the 31 years in the area with no vegetation cover was higher by 7.58°C from wetlands, 7.03°C from forests, 4.1°C from shrublands, and 2.57°C from grasslands. Barren land showed the highest mean value of LST, while shrubs and sparse vegetation cover classes exhibited the lowest mean LSTs (Haylemariyam,

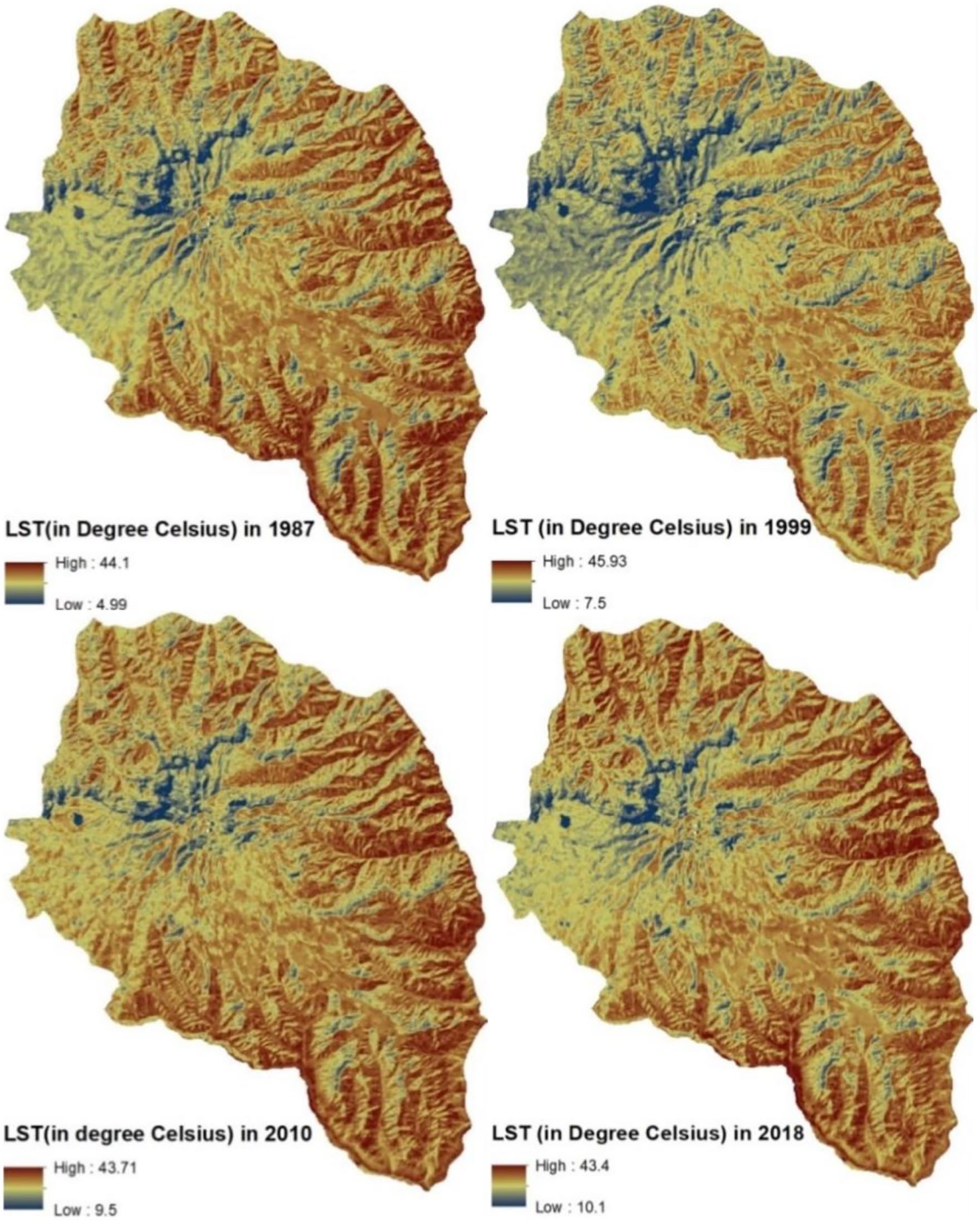

Figure 3. LST distribution of the study watershed.

2018). The LSTs in areas with high human activity intensity like cultivated land were high but low in areas with low intensity of human activity, such as in water bodies, forests, shrublands, and grasslands (Deng et al., 2018; Ullah et al., 2019). Haylemariyam (2018) noted that the LST value of barren land surface exceeds other LUC classes with a mean value of 26.59°C but vegetation covers like shrubs and forests showed the lowest LST values having a mean of 24.57°C.

The result indicates that areas with no vegetation cover were incessantly increasing by 30,499.1 ha over three decades, with a mean of 983.84 ha year^{-1} (Figures 6 and 8). No vegetation areas were increasing by 5,555.2, 13,375.6, and 11,568.3 ha in the first, second, and third periods, respectively. This indicates that on average 462.93, 1,215.96, and 1,446 ha year^{-1} of no vegetation covers were increasing in the first, second, and third periods, respectively. In the third period, the average increment of

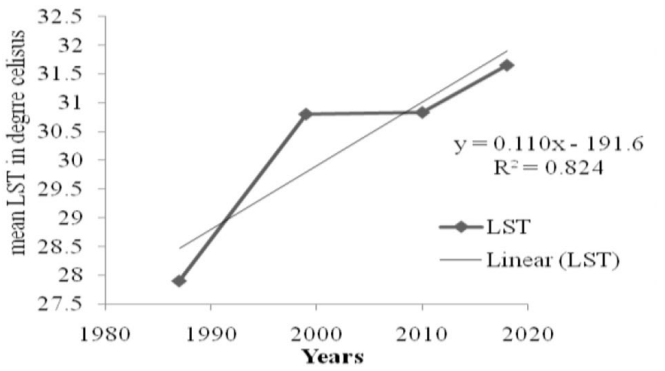

Figure 4. Mean LST in different years at watershed level.

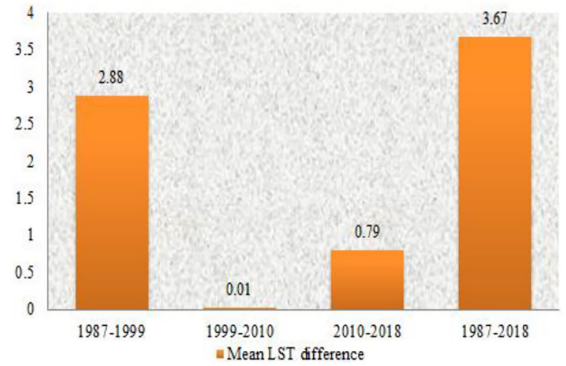

Figure 5. Mean LST difference over different years at watershed level.

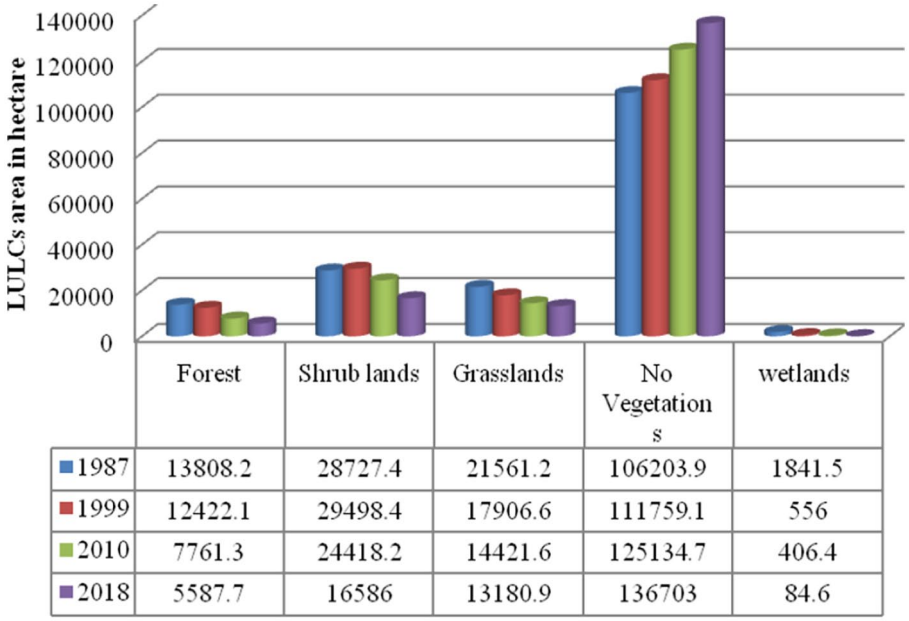

	Forest	Shrub lands	Grasslands	No Vegetations	wetlands
1987	13808.2	28727.4	21561.2	106203.9	1841.5
1999	12422.1	29498.4	17906.6	111759.1	556
2010	7761.3	24418.2	14421.6	125134.7	406.4
2018	5587.7	16586	13180.9	136703	84.6

Figure 6. Proportion of LUCs from 1987 to 2018 (in ha).

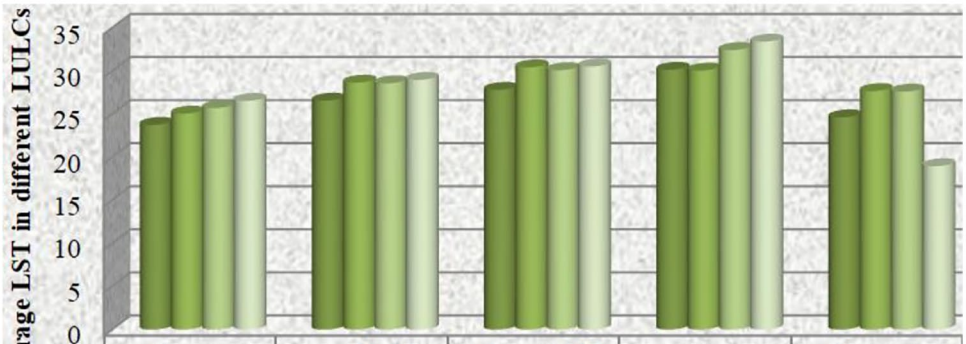

	Forest	Shrublands	Grasslands	No Vegetation	Wetlands
1987	23.75	26.57	27.82	30.15	24.63
1999	25.06	28.66	30.44	30.06	27.68
2010	25.72	28.58	30.11	32.45	27.62
2018	26.54	28.98	30.54	33.42	18.96

Figure 7. LST (in °C) differently in response to LUCs in different years.

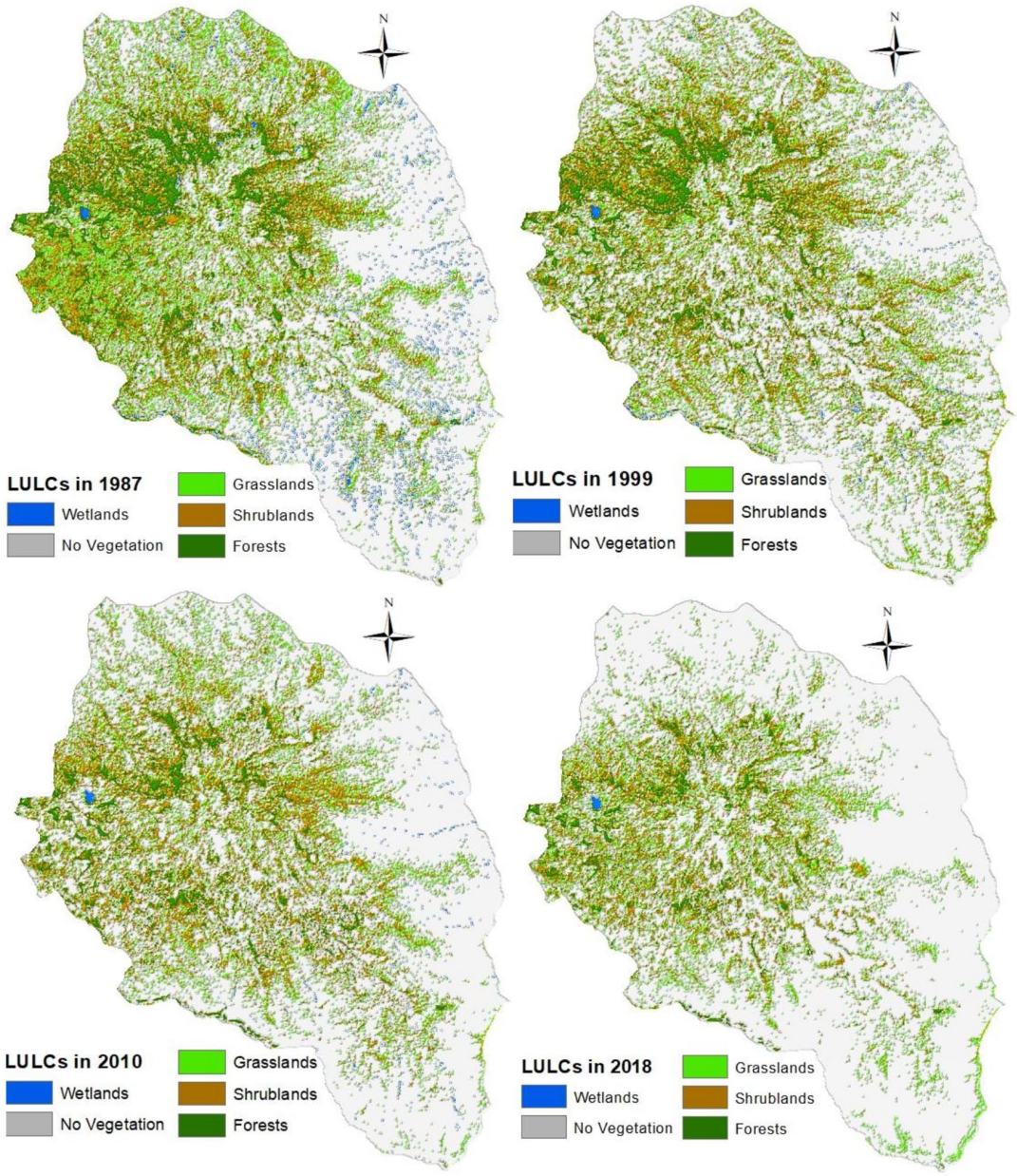

Figure 8. LUCs of the study watershed.

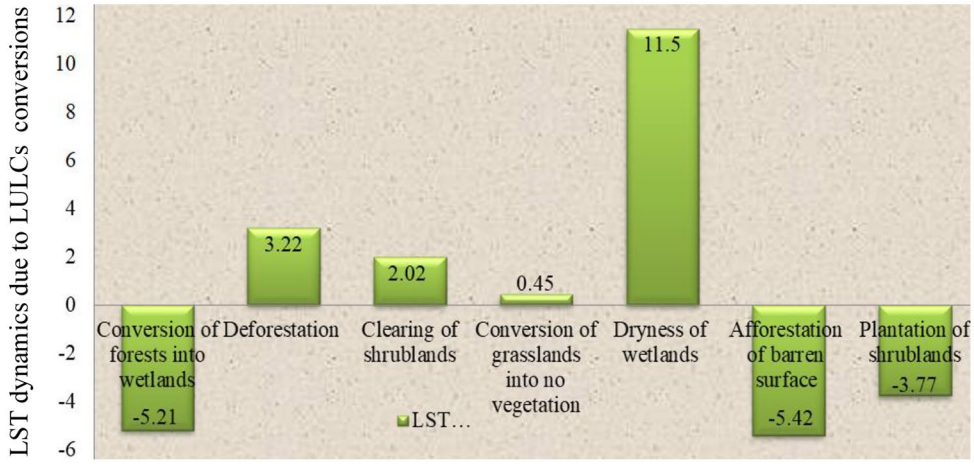

Figure 9. LST dynamics (in °C) over three decades due to conversion from one LUC to others.

Table 3. Conversion of Forest and Shrubs into Other LUCs Like Grasslands and No Vegetation (Such as Croplands).

THE MOST DRIVING FACTORS (%)	FOREST INTO SHRUBLAND, GRASSLANDS	FOREST INTO NO VEGETATION	SHRUBLANDS INTO GRASSLANDS	SHRUBLAND INTO NO VEGETATION	GRASSLANDS INTO NO VEGETATION
Cutting of vegetation biomass	79	7	6	2.8	12.2
Cropland encroachment	2	81	16	77	74
Overgrazing	87.6	14	15	77.5	51
Weak institutional arrangement	73	69	48	66	62

Note. Multiple responses were considered.

no vegetation areas was higher by 983.1 ha year^{-1} for the first and 230 ha year^{-1} for the second period. In the no vegetation area, the average LST was ranging from 30.147°C in 1987 to 33.42°C in 2018, implying that it was increased by 3.05°C over the three decades (Figure 7).

From the total area of the study watershed, wetlands were covered by 1.1% in 1987, 0.32% in 1999, 0.24% in 2010, and 0.05% in 2018. Wetlands were constantly decreasing by 1,756.9 ha over the three decades, with an average of 56.7 ha year^{-1}. They decreased by 1,285.5 ha in the first period, 149.6 ha in the second period, and 321.8 ha in the third period. On average, wetlands declined by 107.125 ha year^{-1} in the first period, 13.6 ha year^{-1} in the second period, and 40.225 ha year^{-1} in the third period. In the first period, the wetlands disappeared by 93.525 ha year^{-1} higher than for the second period and 66.9 ha year^{-1} for the third period. Because of the declining of wetlands coverage, the mean LST of the wetlands was decreasing from 24.63°C in 1987 to 18.96°C in 2018 (Figure 7). In the wetlands, the average LST was 24.72°C over the three decades. The least LST was observed in the wetland ecosystems when compared to other LUCs. Wetland surfaces play an important regulatory role in reducing LST and mitigating thermal effects on the ground (Tan et al., 2020). The distribution of average changes in LST in the water bodies showed the lowest increase than other LUCs followed by forest lands (Hua & Ping, 2018). Despite the enhanced available energy, the average daytime surface temperature in the wetlands was cooler by 5.1°C than the nearby cropland surface temperatures (Stanley, 2018).

Landuse/cover changes and surface temperature dynamics

In the first period, 38.2% of forests changed into other LUCs. Of the total changed, the highest proportion (32%) of forests lost at the gain of shrubs. During the second period, a more transition rate (53.5%) was observed compared to other periods of the study. From this, 44.3% of the forest was changed into shrubs. In the third period, 46.6% of forest lands were lost at the gains of other LUCs. Of this, 30.1% was modified into shrublands. Over the three decades, of the total 72% losses of forests, 40.6%, 17.2%, and 14.2% were converted into shrublands, no vegetation, and grasslands, respectively (Table 4). This may be due to the encroachment of croplands at the expense of grasslands, shrublands, and forests (Assefa & Singh, 2017; Barlow et al., 2016; Liyehu et al., 2019; Twisa & Buchroithner, 2019). The conversion of forests into shrublands and grasslands was driven by cutting live vegetation (ranked by 79%), overgrazing (ranked by 87.6%), and weak institutional arrangement (ranked by 73%) (Table 3). Table 3 indicates that clearing of the forest into no vegetation was also influenced by the encroachment of croplands (rated by 81%) and weak institutional arrangement (ranked by 69%). Expansion of cultivated land and settlements and cutting of vegetation for charcoal production and construction were the most crucial drivers of deforestation (Kindu et al., 2015; Liyehu et al., 2019). Deforestation, removing the natural vegetation cover, leads to soil erosion and ecosystem disturbance, alters surface roughness and reduces evapotranspiration, and increased *albedo* (Yin et al., 2018). Deforestation was the second most contributing factor to the increment of LST by 3.22°C (Figure 9). The increase of LST was largely determined by deforestation (Meseret, 2019). Because of anthropogenic disturbances, deforestation has a significant warming effect in the tropical regions with little seasonality (Danneyrolles et al., 2019; Findell et al., 2017; Muro et al., 2018) since it systematically results in higher radiative fluxes leaving the surface (Duveiller et al., 2018). Deforestation-induced warmer temperatures tend to reduce land carbon, mostly because of increased heterotrophic respiration (Harper et al., 2018). From biophysical and biogeochemical points of view, conversion of forests into croplands, and open lands appears to be the worst land cover transition for climate because it constantly leads to local warming as a result of lower carbon stocks and considerable emission of nitrous oxide and methane (Duveiller et al., 2018).

From the total area, a consistent increasing loss of shrubland was observed at 42.3% in the first, 55% in the second, and 56.3% in the third period (Table 4). In the first period, from 42.3% lost shrubland, 28.3% was cleared for crop production, and 11.5% was developed into the forest. In the second period, from 55% lost shrubland, 29.5%, and 21.8% were cleared to the gain of cultivated lands and grasslands, respectively. Of the

Table 4. Transition Matrix of LUCs in Abaminus Watershed Between 1987 and 2018 (Unit: Hectare).

PERIODS	LUCS	CHANGED LAND USE/COVERS					LOSSES (%)
		WETLANDS (%)	NO-VEGETATION (%)	GRASSLANDS (%)	SHRUBS (%)	FORESTS (%)	
1987–1999	Wetlands	13.3	78.5	4.4	3.4	0.4	86.7
	No-vegetation	0.3	84.5	8.4	6.1	0.7	15.5
	Grasslands	0.1	55.5	21.3	20.9	2.2	78.7
	Shrubs	0.1	28.3	2.4	57.7	11.5	42.3
	Forests	0.1	3	3.1	32	61.8	38.2
1999–2010	Wetlands	36.4	59.9	0.6	1.4	1.7	63.6
	No-vegetation	0.2	92.2	4.4	2.5	0.7	7.8
	Grasslands	0	63.3	21.9	13.9	0.9	78.1
	Shrubs	0	29.5	21.8	45	3.7	55
	Forests	0	4.7	4.5	44.3	46.5	53.5
2010–2018	Wetlands	15.2	84.5	0.1	0.1	0.1	84.8
	No-vegetation	0	94.8	3.8	1.2	0.2	5.2
	Grasslands	0	63.4	23.7	12.4	0.5	76.3
	Shrubs	0	27.9	23.5	43.7	4.9	56.3
	Forests	0	13.3	3.2	30.1	53.4	46.6
1987–2018	Wetlands	3.4	94.5	0.8	0.9	0.4	96.6
	No-vegetation	0	93.8	3.6	2.2	0.4	6.2
	Grasslands	18.9	61.8	10.6	7.7	1	89.4
	Shrubs	0	53.8	20.2	22.3	3.7	77.7
	Forests	0	17.2	14.2	40.6	28	72

total lost shrublands, 27.9% were cleared into croplands, followed by 23.5% were converted into grasslands in the third period. Over the three decades, from 77.7% lost shrublands, 53.8% were cleared into no vegetation (croplands) and 20.25% were modified into grasslands. This agrees with the expansion of cultivated lands at the expense of shrublands (Barlow et al., 2016; Liyehu et al., 2019; Twisa & Buchroithner, 2019). Cropland expansion and overgrazing due to the weak institutional arrangement were the major driving factors for the clearing of shrublands into no vegetation (Table 3). The clearing of shrublands caused an increase of LST by 2.02°C over the three decades (Figure 9). Changing shrublands alter the radiative and non-radiative properties of the land surfaces (Duveiller et al., 2018).

The grasslands were decreased by 78.7% in the first, 78.1% in the second, and 76.3% in the third period. The highest loss was observed in the first period. During this period, from the total 78.7% lost, 55.5% changed into croplands, and 20.9% converted into shrublands (Table 4). This further implies that 4.3% and 1.61% of the grasslands were lost to the gain of croplands and shrublands per year, respectively. Of the total lost area, 63.3% was changed into cropland and 13.9% was converted into shrubland in the second period. In the third period, 63.4% changed into cropland and 12.4% changed into shrubland. An area covered with grassland was lost by 89.4% of the gain of other LUCs over the three decades. Of the total lost, 61.8% was cleared into no vegetation cover (Table 4). The grassland can be converted into no-vegetation, including croplands and barren surfaces due to overgrazing (highly rated 77.5%) and weak institutional arrangements, highly rated by 76% (Table 3). The results of this study agree with the encroachment of croplands at the expense of grasslands (Assefa & Singh, 2017; Liyehu et al., 2019; Twisa & Buchroithner, 2019). Clearing of grasslands into barrenland and the soil surface contributed to increasing LSTs by 0.45°C (Figure 9). The conversion of grasslands into croplands has consistently reduced the amount of energy available for evapotranspiration whilst brightening the surface (Duveiller et al., 2018).

The largest area of the wetlands was converted into no-vegetation. From the total lost area of the wetlands, 78.5% (in the

Table 5. The Most Driving Factors for the Conversion of One Land Cover into Another.

PRINCIPAL DRIVING FACTORS	WETLANDS INTO GRASSLANDS (%)	WETLANDS INTO NO VEGETATION (%)	WETLANDS INTO SHRUBLANDS (%)
Sedimentation	71	21	8
Rising of temperature	24.4	66.1	11.5
Drainage for irrigated croplands	14.3	83.6	2.1
Weak institutional arrangement	19	73	8
Recurrent drought	29.4	33.5	38.1
PRINCIPAL DRIVING FACTORS	**NO-VEGETATION INTO GRASSLANDS (%)**	**NO VEGETATION INTO SHRUBLANDS, FORESTS (%)**	**NO VEGETATION INTO WETLANDS (%)**
Enabled institutional arrangement	45	71.7	53.3
Fallowing practice	76.3	14.4	8.6
Enclosure management	64.3	24.3	72.4
Plantation of different plant species	5.6	89.1	5.3

Note. Multiple responses were considered.

first period), 59.9% (in the second period), and 84.5% (in the third period) were converted into no-vegetation. The result indicates that the largest lost area of wetlands at the gain of no-vegetation was observed in the third period when compared to the first and second periods. Of the total lost area of the wetlands (96.6%), 94.5% were to the gains of no-vegetation over the three decades (Table 4) due to drainage for irrigated croplands (83.6% highly rated), sedimentation (71% highly rated), and weak institutional principles and arrangement (73 % highly rated) (Table 5). Loss of wetlands or water surface changes over time were the major environmental degradation indicators mainly identified in the arid environment (Hadeel et al., 2011). Figure 9 reveals that wetland disappearance contributed to the increment of LST by 11.5°C over 31 years, implying that on average 0.37°C $year^{-1}$ due to wetlands losing. Despite a decline in methane oxidation emission following wetland drainage, conversion of wetlands into cropland results in a considerable net increase in land surface temperature or heat-trapping (Muro et al., 2018). Anthropogenic disturbance and rising LST have great effects on the status of wetlands changing their hydrological and evapotranspiration regimes (Muro et al., 2018), and carbon storage (Moomaw et al., 2018). Drainage and drying of wetland soils increase microbial decomposition of stored organic carbon and cause to emit significant amounts of this stored natural carbon into the atmosphere and reduce the ability of wetlands to sequester additional carbon (Pendleton et al., 2012). Preventing further wetland loss is found to be crucial to protect carbon stores and in limiting future emissions to meet climate goals, but is seldom considered (Moomaw et al., 2018). Moomaw et al. (2018) further noted that wetlands are among the most carbon-rich sinks on the planet sequestering approximately as much carbon as do global forest ecosystems.

The area with no vegetation was covered by 3.6% of grasslands, 2.2% of shrublands, and 0.4% of forest over the three decades (Table 4). From the total planted area, an area with no vegetation was vegetated by 8.4% grasslands and 6.1% shrublands in the first period; by 4.4% grasslands, and 2.3% shrublands in the second; and by 8% grasslands and 1.2% shrublands in the third period. This indicates that the largest area with no vegetation was consistently covered by grasslands, followed by shrublands. Table 5 indicates that from the total respondents, 76.3% reported that fallow practice was the most important factor to change cultivated and barren land surfaces into grasslands. Of the total, 89.1% reported, plantation of eucalyptus and other exotic plant species on unproductive croplands and degraded communal lands was rated a highly important factor in the conversion of no vegetation into shrublands (Table 5). A realistic representation of the Spatio-temporal dynamics of key land-use practices, such as fallowing, and abandonment of land, afforestation, and reforestation is one of the priorities of earth system modeling (Chen et al., 2019). Figure 9 reveals that the plantation of shrubs and trees has also contributed to the decrease of LST by 3.77°C, with an average rate of 0.12°C $year^{-1}$. Thomas et al. (2018) reported that daytime air temperatures under shrubs and trees were cooler compared with other LUCs areas.

Afforestation is being changed of other LUCs into forested areas (Hu et al., 2019). Afforestation of soil and the barren surface has contributed to the decline of LST by 5.42°C, on average, by 0.17°C $year^{-1}$ (Figure 9). The mean LST of green space was 3°C lower than impervious and barren soil surface, implying the important role of plantation practice in mitigating surface temperature (Estoque et al., 2017). Forests can serve as a thermal insulator compared with open areas and such buffering effect has the potential to reduce the severe impacts

of climate change on the forest ecosystem (De Frenne et al., 2019). Re-/afforestation as local mitigation and adaptation measures could be an attractive strategy because of the increasing annual cooling effects of forest cover (Bright et al., 2017). Afforestation/reforestation, and avoiding deforestation encourage carbon capture and storage; can support large-scale carbon dioxide (CO_2) removal from the atmosphere to limit global warming to below 2°C by 2,100 (Harper et al., 2018). Reducing emissions from tropical deforestation and forest biomass degradation is beneficial for climate mitigation for both biogeochemical and biophysical reasons (Duveiller et al., 2018; Syktus & McAlpine, 2016). Syktus and McAlpine (2016) noted that restoration of forest and shrubland biomass triggers a positive feedback loop between the land surface and the atmosphere by increasing an evaporative fraction (proportion of latent heat flux relative to the sensible heat flux), eddy dissipation, and turbulent mixing in the boundary-layer resulting in the enhanced cloud formation and precipitation over the restored areas.

Restoration of wetlands decreased LST by 5.21°C, implying that on an average decline of 0.17°C $year^{-1}$. The conversion of the bare surface into water bodies reduced surface temperatures by 4.5°C in Zimbabwe (Mushore et al., 2017). Water bodies play a significant regulatory role in reducing LST and mitigating thermal effects on the ground (Tan et al., 2020). Tracts of open water between the patches of wetland vegetation could delay heat exchange with the atmosphere and keep temperature cooling that helps counteract rising temperatures on a local scale (Stanley, 2018). Preventing and restoring wetland ecosystems can regenerate their ability to remove and sequester CO_2 from the atmosphere (Moomaw et al., 2018). Wetland restoration has significant implications for an atmospheric carbon cycle (C-cycle) because a substantial portion of the soil carbon pool is stored in the wetlands (Moomaw et al., 2018).

Conclusion

Retrieving LST from satellite data fills the knowledge gap in the local-scale temperature effects of different landscape characters and biophysical changes induced by anthropogenic activities. Thus, the study was to investigate the impact of land use/cover changes on the dynamics of land surface temperature over the Abaminus watershed, Northwest Ethiopia. The results disclosed that the mean LST was increased by 3.67°C in the watershed, 2.79°C in the forest cover, 2.4°C in the shrublands, 2.72°C in the grasslands, and 3.05°C in no vegetation area over 31 years. Over the study period, the mean LST was increased by 11.5°C, 3.22°C, and 2.02°C on account of wetlands loss, deforestation, and clearing of shrublands in that order. Besides, clearing of grasslands into the barren surface has also contributed to the increase of LST by 0.45°C. Cultivated land encroachment and overgrazing due to weak institutional arrangements were the major factors of vegetation clearing, resulting in LST increments. Wetland loss was largely caused by high drainage for irrigated croplands, sedimentation, and weak institutional arrangement. Conversely, the LST was decreased by 5.42°C and 3.77°C on the afforested barren surfaces and planted shrublands, respectively over 31 years. Therefore, it is concluded that enabling institutional arrangement should be employed to control the cutting of live and dead vegetation, and encroachment of cultivated lands. Moreover, enclosure management and plantation of multipurpose species on degraded communal lands shall be scaled-up to significantly reduce land surface temperature.

Author Contributions

The first author initiated the research idea, reviewed relevant literature, designed the methods, conducted field data collection, performed data cleaning, analyzed the data, interpretation, and prepare draft manuscripts for publication. Co-authors evaluated the research idea, supervised the whole research activities, and developed the manuscript. All authors read and approved the final manuscript.

Availability of Data and Material

The data generated and processed in this manuscript were included in the manuscript submission. Further data will be provided upon the request of the corresponding author.

Declaration of Conflicting Interests

The author(s) declared no potential conflicts of interest with respect to the research, authorship, and/or publication of this article.

Funding

The author(s) received no financial support for the research, authorship, and/or publication of this article.

Ethics Approval and Consent to Participate

All authors approve to publish the findings, and there is no ethical conflict.

Consent for Publication

All authors read the manuscript and agreed to publication.

ORCID iD

Mesfin Anteneh https://orcid.org/0000-0003-1657-7413

REFERENCES

Ahmed, B., Kamruzzaman, M., Zhu, X., Rahman, M., & Choi, K. (2013). Simulating land cover changes and their impacts on land surface temperature in Dhaka, Bangladesh. *Remote Sensing*, 5(11), 5969–5998. https://doi.org/10.3390/rs5115969

Assefa, A., & Singh, K. N. (2017). The implications of land use and land cover changes for rural household food insecurity in the northeastern highlands of Ethiopia: The case of the Teleyayen sub-watershed. *Agriculture & Food Security*, 6, 56. https://doi.org/10.1186/s40066-017-0134-4

Bai, Z. G., Dent, D. L., Olsson, L., & Schaepman, M. E. (2008). Proxy global assessment of land degradation. *Soil Use and Management*, 24(3), 223–234. https://doi.org/10.1111/j.1475-2743.2008.00169.x

Balew, A., & Korme, T. (2020). Monitoring land surface temperature in Bahir Dar city and its surrounding using Landsat images. *The Egyptian Journal of Remote Sensing and Space Science*, 23, 371–386. https://doi.org/10.1016/j.ejrs.2020.02.001

Barlow, J., Lennox, G. D., Ferreira, J., Berenguer, E., Lees, A. C., Mac Nally, R., Thomson, J. R., Ferraz, S. F., Louzada, J., Oliveira, V. H., Parry, L., Solar, R. R.,

Vieira, I. C., Aragão, L. E., Begotti, R. A., Braga, R. F., Cardoso, T. M., de Oliveira, R. C. Jr., Souza, C. M. Jr., . . . Gardner, T. A. (2016). Anthropogenic disturbance in tropical forests can double biodiversity loss from deforestation. *Nature*, 535(7610), 144–147. https://doi.org/10.1038/nature18326

Barsi, J. A., Schott, J. R., Palluconi, F. D., & Hook, S. J. (2005). *Validation of a web-based atmospheric correction tool for single thermal band instruments* [Conference session]. Proceedings SPIE, 58820 E, Bellingham, WA, p. 7.

Birhanu, A., Masih, I., van der Zaag, P., Nyssen, J., & Cai, X. (2019). Impacts of land use and land cover changes on hydrology of the Gumara catchment, Ethiopia. *Physics and Chemistry of the Earth*, 112, 165–174.

Bright, R. M., Davin, E., O'Halloran, T., Pongratz, J., Zhao, K., Cescatti, A., & Halloran, D. O. (2017). Local temperature response to land cover and management change driven by non-radiative processes. *Nature Climate Change*, 7, 296–302. https://doi.org/10.1038/nclimate3250

Brovkin, V., Boysen, L., Arora, V. K., Boisier, J. P., Cadule, P., Chini, L., Claussen, M., Friedlingstein, P., Gayler, V., van Den Hurk, B. J. J. M., Hurtt, G. C., Jones, C. D., Kato, E., de Noblet-Ducoudré, N., Pacifico, F., Pongratz, J., & Weiss, M. (2013). Effect of anthropogenic land-use and land-cover changes on climate and land carbon storage in CMIP5 projections for the twenty-first century. *Journal of Climate*, 26(18), 6859–6881. https://doi.org/10.1175/jcli-d-12-00623.1

Butt, A., Shabbir, R., Ahmad, S. S., & Aziz, N. (2015). Land use change mapping and analysis using remote sensing and GIS: A case study of Simly watershed, Islamabad, Pakistan. *The Egyptian Journal of Remote Sensing and Space Science*, 18, 251–259. https://doi.org/10.1016/j.ejrs.2015.07.003

Campos, J. C., Sillero, N., & Brito, J. C. (2012). Normalized difference water indexes have dissimilar performances in detecting seasonal and permanent water in the Sahara–Sahel transition zone. *Journal of Hydrology*, 464–465, 438–446. https://doi.org/10.1016/j.jhydrol.2012.07.042

Chander, G., & Markham, B. (2003). Revised Landsat-5 TM radiometric calibration procedures and post-calibration dynamic ranges. *IEEE Transactions on Geoscience and Remote Sensing*, 41(11), 2674–2677. https://doi.org/10.1109/tgrs.2003.818464

Chander, G., Markham, B. L., & Helder, D. L. (2009). Summary of current radiometric calibration coefficients for Landsat MSS, TM, ETM+, and EO-1 ALI sensors. *Remote Sensing of Environment*, 113, 893–903. https://doi.org/10.1016/j.rse.2009.01.007

Chatterjee, R. S., Singh, N., Thapa, S., Sharma, D., & Kumar, D. (2017). Retrieval of land surface temperature (LST) from Landsat TM6 and TIRs data by single channel radiative transfer algorithm using satellite and ground-based inputs. *International Journal of Applied Earth Observation and Geoinformation*, 58, 264–277. https://doi.org/10.1016/j.jag.2017.02.017

Chen, C., Park, T., Wang, X., Piao, S., Xu, B., Chaturvedi, R. K., Fuchs, R., Brovkin, V., Ciais, P., Fensholt, R., Tømmervik, H., Bala, G., Zhu, Z., Nemani, R. R., & Myneni, R. B. (2019). China and India lead in greening of the world through land-use management. *Nature Sustainability*, 2, 122–129. https://doi.org/10.1038/s41893-019-0220-7

Danneyrolles, V., Dupuis, S., Fortin, G., Leroyer, M., de Römer, A., Terrail, R., Vellend, M., Boucher, Y., Laflamme, J., Bergeron, Y., & Arseneault, D. (2019). Stronger influence of anthropogenic disturbance than climate change on century-scale compositional changes in northern forests. *Nature Communications*, 10, 1265. https://doi.org/10.1038/s41467-019-09265-z

Debie, E., Singh, K. N., & Belay, M. (2019). Effect of conservation structures on curbing rill erosion in micro-watersheds, northwest Ethiopia. *International Soil and Water Conservation Research*, 7, 239–247. https://doi.org/10.1016/j.iswcr.2019.06.001

De Frenne, P., Zellweger, F., Rodríguez-Sánchez, F., Scheffers, B. R., Hylander, K., Luoto, M., Vellend, M., Verheyen, K., & Lenoir, J. (2019). Global buffering of temperatures under forest canopies. *Nature Ecology & Evolution*, 3(5), 744–749. https://doi.org/10.1038/s41559-019-0842-1

Deng, Y., Wang, S., Bai, X., Tian, Y., Wu, L., Xiao, J., Chen, F., & Qian, Q. (2018). Relationship among land surface temperature and LUCC, NDVI in typical Karst area. *Scientific Reports*, 8, 641. https://doi.org/10.1038/s41598-017-19088-x

Deng, Y., Wu, C., Li, M., & Chen, R. (2015). RNDSI: A ratio normalized difference soil index for remote sensing of urban/suburban environments. *International Journal of Applied Earth Observation and Geoinformation*, 39, 40–48. https://doi.org/10.1016/j.jag.2015.02.010

Dinka, M. O., & Chaka, D. D. (2019). Analysis of land use/land cover change in Adei watershed, Central Highlands of Ethiopia. *Journal of Water and Land Development*, 41(1), 146–153. https://doi.org/10.2478/jwld-2019-0038

Duan, Z., & Bastiaanssen, W. G. (2013). Estimating water volume variations in lakes and reservoirs from four operational satellite altimetry databases and satellite imagery data. *Remote Sensing of Environment*, 134, 403–416. https://doi.org/10.1016/j.rse.2013.03.010

Duveiller, G., Hooker, J., & Cescatti, A. (2018). The mark of vegetation change on Earth's surface energy balance. *Nature Communications*, 9, 679. https://doi.org/10.1038/s41467-017-02810-8

Ellis, E. C., Antill, E. C., & Kreft, H. (2012). All is not loss: Plant biodiversity in the anthropocene. *PLoS One*, 7, e30535. https://doi.org/10.1371/journal.pone.0030535

Ermida, S. L., DaCamara, C. C., Trigo, I. F., Pires, A. C., Ghent, D., & Remedios, J. (2017). Modelling directional effects on remotely sensed land surface temperature. *Remote Sensing of Environment*, 190, 56–69. https://doi.org/10.1016/j.rse.2016.12.008

Estoque, R. C., Murayama, Y., & Myint, S. W. (2017). Effects of landscape composition and pattern on land surface temperature: An urban heat island study in the megacities of Southeast Asia. *The Science of the Total Environment*, 577, 349–359. https://doi.org/10.1016/j.scitotenv.2016.10.195

Findell, K. L., Berg, A., Gentine, P., Krasting, J. P., Lintner, B. R., Malyshev, S., Santanello, J. A. Jr., & Shevliakova, E. (2017). The impact of anthropogenic land use and land cover change on regional climate extremes. *Nature Communications*, 8(1), 989. https://doi.org/10.1038/s41467-017-01038-w

Gašparović, M., Zrinjski, M., & Gudelj, M. (2019). Automatic cost-effective method for land cover classification (ALCC). *Computers, Environment and Urban Systems*, 76, 1–10. https://doi.org/10.1016/j.compenvurbsys.2019.03.001

Genesis, T. Y., David, D., Olsson, L., Anna, E., Compton, T., & Tucker, J. III. (2015). *Use of the Normalized Difference Vegetation Index (NDVI) to assess land degradation at multiple scales of current status, future trends, and practical considerations*. Springer, Heidelberg, Dordrecht.

Gessesse, B., & Bewket, W. (2014). Drivers and implications of land use and land cover change in the central Highlands of Ethiopia: Evidence from remote sensing and socio-demographic data integration. *EJOSSAH*, X(2), 1-23. https://www.researchgate.net/publication/337649589

Gogoi, P. P., Vinoj, V., Swain, D., Roberts, G., Dash, J., & Tripathy, S. (2019). Land use and land cover change effect on surface temperature over eastern India. *Scientific Reports*, 9, 8859. https://doi.org/10.1038/s41598-019-45213-z

Grover, A., & Singh, R. (2015). Analysis of urban heat island (UHI) in relation to Normalized Difference Vegetation Index (NDVI): A comparative study of Delhi and Mumbai. *Environments*, 2(4), 125–138. https://doi.org/10.3390/environments2020125

Hadeel, A., Jabbar, M., & Chen, X. (2011). Remote sensing and GIS application in the detection of environmental degradation indicators. *Geo-spatial Information Science*, 14(1), 39–47. https://doi.org/10.1007/s11806-011-0441-z

Harper, A. B., Powell, T., Cox, P. M., House, J., Huntingford, C., Lenton, T. M., Sitch, S., Burke, E., Chadburn, S. E., Collins, W. J., Comyn-Platt, E., Daioglou, V., Doelman, J. C., Hayman, G., Robertson, E., van Vuuren, D., Wiltshire, A., Webber, C. P., Bastos, A., . . . Shu, S. (2018). Land-use emissions play a critical role in land-based mitigation for Paris climate targets. *Nature Communications*, 9, 2938. https://doi.org/10.1038/s41467-018-05340-z

Haylemariyam, M. B. (2018). Detection of land surface temperature in relation to land use land cover change: Dire Dawa city, Ethiopia. *Journal of Remote Sensing & GIS*, 7, 245. https://doi.org/10.4172/2469-4134.1000245

He, C., Gao, B., Huang, Q., Ma, Q., & Dou, Y. (2017). Environmental degradation in the urban areas of China: Evidence from multi-source remote sensing data. *Remote Sensing of Environment*, 193(2017), 65–75.

Hu, P., Zhang, W., Xiao, L., Yang, R., Xiao, D., Zhao, J., Wang, W., Chen, H., & Wang, K. (2019). Moss-dominated biological soil crusts modulate soil nitrogen following vegetation restoration in a subtropical Karst region. *Geoderma*, 352, 70–79. https://doi.org/10.1016/j.geoderma.2019.05.047

Hua, A. K., & Ping, O. W. (2018). The influence of land-use/land-cover changes on land surface temperature: A case study of Kuala Lumpur Metropolitan city. *European Journal of Remote Sensing*, 51(1), 1049–1069. https://doi.org/10.1080/22797254.2018.1542976

Hurni, H., Debele, B., Zeleke, G., Abate, S., Bantider, A., Portner, B., Yitaferu, B., & Ludi, E. (2010). Land degradation and sustainable land management in the highlands of Ethiopia. In H. Hurni & U. Wiesmann (Eds.), *Global change and sustainable development: A synthesis of regional experiences from research partnerships. Perspectives of the Swiss National Centre of competence in Research (NCCR) North-South, University of Bern* (Vol. 5, pp. 187–207). Geographica Bernensia.

Jain, M., Dimri, A., & Niyogi, D. (2017). Land-air interactions over urban-rural transects using satellite observations: Analysis over Delhi, India from 1991–2016. *Remote Sensing*, 9, 1283–1314. https://doi.org/10.3390/rs9121283

Jia, G., Shevliakova, E., Artaxo, P., De Noblet-Ducoudré, N., Houghton, R., House, J., Kitajima, K., Lennard, C., Popp, A., Sirin, A., Sukumar, R., & Verchot, L. (2019). Land–climate interactions. In P. R. Shukla, J. Skea, E. Calvo Buendia, V. Masson-Delmotte, H. O. Pörtner, D. C. Roberts, P. Zhai, R. Slade, S. Connors, R. van Diemen, M. Ferrat, E. Haughey, S. Luz, S. Neogi, M. Pathak, J. Petzold, J. Portugal Pereira, P. Vyas, E. Huntley, … J. Malley (Eds.), *Climate change and land: An IPCC special report on climate change, desertification, land degradation, sustainable land management, food security, and greenhouse gas fluxes in terrestrial ecosystems* (pp. 131-205). In press.

Kindu, M., Schneider, T., Teketay, D., & Knoke, T. (2015). Drivers of land use/land cover changes in Munessa-Shashemene landscape of the south-central highlands

of Ethiopia. *Environmental Monitoring and Assessment*, 187, 452. https://doi.org/10.1007/s10661-015-4671-7

Kleemann, J., Baysal, G., Bulley, H. N. N., & Fürst, C. (2017). Assessing driving forces of land use and land cover change by a mixed-method approach in north-eastern Ghana, West Africa. *Journal of Environmental Management*, 196, 411–442. https://doi.org/10.1016/j.jenvman.2017.01.053

Lai, Y. J., Li, C. F., Lin, P. H., Wey, T. H., & Chang, C. S. (2012). Comparison of MODIS land surface temperature and ground-based observed air temperature in complex topography. *International Journal of Remote Sensing*, 33(24), 7685–7702. https://doi.org/10.1080/01431161.2012.700422

Lee, L., Chen, L., Wang, X., & Zhao, J. (2011). *Use of Landsat TM/ETM+ data to analyze urban heat island and its relationship with land use/cover change* [Conference session]. 2011 International Conference on Remote Sensing, Environment, and Transportation Engineering. IEEE, Nanjing, China, pp. 922–927. https://doi.org/10.1109/RSETE.2011.5964429

Li, H., Wang, C., Zhong, C., Su, A., Xiong, C., Wang, J., & Liu, J. (2017). Mapping urban bare land automatically from Landsat imagery with a simple index. *Remote Sensing*, 9, 249. https://doi.org/10.3390/rs9030249

Li, Z. L., Tang, B. H., Wu, H., Ren, H., Yan, G., Wan, Z., Trigo, I. F., & Sobrino, J. A. (2013). Satellite-derived land surface temperature: Current status and perspectives. *Remote Sensing of Environment*, 131, 14–37. https://doi.org/10.1016/j.rse.2012.12.008

Liang, S., Wang, D., He, T., & Yu, Y. (2019). Remote sensing of earth's energy budget: Synthesis and review. *International Journal of Digital Earth*, 12(7), 737–780. https://doi.org/10.1080/17538947.2019.1597189

Liyehu, M., Tsunekaw, A., Haregeweyn, N., Tsegaye, D., Adgo, E., Tsubo, M., Masunag, T., Almaw, A., Sultan, D., & Yibeltal, M. (2019). Exploring land use/land cover changes, drivers and their implications in contrasting agro-ecological environments of Ethiopia. *Land Use Policy*, 87, 104052. https://doi.org/10.1016/j.landusepol.2019.104052

Majumder, A., Kingra, P. K., Setia, R., Singh, S. P., & Pateriya, B. (2020). Influence of land use/land cover changes on surface temperature and its effect on crop yield in different agro-climatic regions of Indian Punjab. *Geocarto International*, 35(6), 663–686. https://doi.org/10.1080/10106049.2018.1520927

Meseret, M. (2019). Analysis of spatio-temporal land surface temperature and normalized difference vegetation index changes in the Andassa watershed, Blue Nile Basin, Ethiopia. *Journal of Resources and Ecology*, 10(1), 77–85. https://doi.org/10.5814/j.issn.1674-764x.2019.01.010

Moomaw, W. R., Chmura, G. L., Davies, G. T., Finlayson, C. M., Middleton, B. A., Natali, S. M., Perry, J. E., Roulet, N., & Sutton-Grier, A. E. (2018). Wetlands in a changing climate: Science, policy, and management. *Wetlands*, 38, 183–205. https://doi.org/10.1007/s13157-018-1023-8

Muro, J., Strauch, A., Heinemann, S., Steinbach, S., Thonfeld, F., Waske, B., & Diekkrüger, B. (2018). Land surface temperature trends as indicator of land use changes in wetlands. *International Journal of Applied Earth Observation and Geoinformation*, 70, 62–71. https://doi.org/10.1016/j.jag.2018.02.002

Mushore, T. D., Mutanga, O., Odindi, J., & Dube, T. (2017). Linking major shifts in land surface temperatures to long term land use and land cover changes: A case of Harare, Zimbabwe. *Urban Climate*, 20, 120–134. https://doi.org/10.1016/j.uclim.2017.04.005

Pal, S., & Ziaul, S. (2017). Detection of land use and land cover change and land surface temperature in English Bazar urban centre. *The Egyptian Journal of Remote Sensing and Space Science*, 20(1), 125–145. https://doi.org/10.1016/j.ejrs.2016.11.003

Pendleton, L., Donato, D. C., Murry, B. C., Crooks, S., Jenkins, W. A., Sifleet, S., Craft, C., Fourqurean, J. W., Kauffman, J. B., Marba, N., Megonigal, J. P., Pidgeon, E., Herr, D., Gordon, D., & Baldera, A. (2012). Estimating global 'blue carbon' emissions from conversion and degradation of vegetated coastal ecosystems. *PLoS One*, 7(9), e43542. https://doi.org/10.1371/journal.pone.0043542

Pandey, S. K, Vinoj, V., Landu, K., & Babus, SS. (2017). Declining pre-monsoon dustloading over south Asia: Signature of a changing regional climate. *Scientific Reports* 7, 1-10. https://doi.org/10.1038/s41598-017-16338

Peng, W., Zhou, J., Xue, S., & Dong, L. (2017). Land surface temperature and its impact factors in western Sichuan plateau, China. *Geocarto International*, 32(8), 919-934.

Poulin, B., Davranche, A., & Lefebvre, G. (2010). Ecological assessment of Phragmites australis wetlands using multi-season spot-scenes. *Remote Sensing of Environment*, 114, 1602–1609. https://doi.org/10.1016/j.rse.2010.02.014

Reddy, A. S., & JangaReddy, M. (2013). NDVI based assessment of land use land cover dynamics in a rain-fed watershed using remote sensing and GIS. *International Journal of Scientific and Engineering Research*, 4(12), 87-93.

Rogers, A. S., & Kearney, M. S. (2004). Reducing signature variability in unmixing coastal marsh thematic mapper scenes using spectral indices. *International Journal of Remote Sensing*, 25, 2317–2335.

Sinha, S., Sharma, L. K., & Nathawat, M. S. (2015). Improved land use land cover classification of semi-arid deciduous forests landscapes using thermal remote sensing. *The Egyptian Journal of Remote Sensing and Space Science*, 18, 217–233. https://doi.org/10.1016/j.ejrs.2015.09.005

Sobrino, J. A., Jimenez-Munoz, J., & Paolini, L. (2004). Land surface temperature retrieval from Landsat™-5. *Remote Sensing of Environment*, 90, 434–440. https://doi.org/10.1016/j.rse.2004.02.003

Soti, V., Tran, A., Bailly, J. S., Puech, C., Seen, D. L., & Begue, A. (2009). Assessing optical earth observation systems for mapping and monitoring temporary ponds in arid areas. *International Journal of Applied Earth Observation and Geoinformation*, 11, 344–351. https://doi.org/10.1016/j.jag.2009.05.005

Stanley, S. (2018), Restored wetlands could lower local surface temperatures, *Eos*, 99. https://doi.org/10.1029/2018EO103203

Syktus, J., & McAlpine, C. A. (2016). More than carbon sequestration: Biophysical climate benefits of restored savannas woodlands. *Scientific Reports*, 6, 29194. https://doi.org/10.1038/srep29194

Tan, J., Yu, D., Li, Q., Tan, X., & Zhou, W. (2020). The spatial relationship between land use/cover change and land surface temperature in the Dongting Lake area, China. *Scientific Reports*, 10, 9245. https://doi.org/10.1038/s41598-020-66168-6

Thomas, A. D., Elliott, D. R., Dougill, A. J., Stringer, L. C., Hoon, S. R., & Sen, R. (2018). The influence of trees, shrubs, and grasses on microclimate, soil carbon, nitrogen, and CO_2 efflux: Potential implications of shrub encroachment for Kalahari rangelands. *Land Degradation and Development*, 29, 1306–1316. https://doi.org/10.1002/ldr.2918

Twisa, S., & Buchroithner, M. F. (2019). Land use and land cover change detection in warm river basin, Tanzania. *Land*, 8, 136. https://doi.org/10.3390/land8090136

Ullah, S., Tahir, A. A., Akbar, T. A., Hassan, Q. K., Dewan, A., Khan, A. J., & Khan, M. (2019). Remote sensing-based quantification of the relationships between land use/land cover changes and surface temperature over the lower Himalayan region. *Sustainability*, 11, 5492. https://doi.org/10.3390/su11195492

USGS. (2016). *Landsat 8 data users handbook*. Department of the Interior, U.S. Geological Survey.

Weng, Q. (2009). Thermal infrared remote sensing for urban climate and environmental studies: Methods, applications, and trends. *ISPRS Journal of Photogrammetry and Remote Sensing*, 64, 335–344. https://doi.org/10.1016/j.isprsjprs.2009.03.007

Wenga, Q., Lub, D., & Schubring, J. (2004). Estimation of land surface temperature vegetation abundance relationship for urban heat island studies. *Remote Sensing of Environment*, 89, 467–483.

Xian, G., Homer, C., & Fry, J. (2009). Updating the 2001 national land cover database land cover classification to 2006 by using Landsat imagery change detection methods. *Remote Sensing of Environment*, 113, 1133–1147. https://doi.org/10.1016/j.rse.2009.02.004

Xiao, R., Weng, Q., Ouyang, Z., Li, W., Schienke, E. W., & Zhang, Z. (2008). Land surface temperature variation and major factors in Beijing, China. *Photogrammetric Engineering & Remote Sensing*, 74(4), 451–461.

Xie, Y., Shal, Z., & Yu, M. (2008). Remote sensing imagery in vegetation mapping: A review. *Journal of Plant Ecology*, 1(1), 9–23. https://doi.org/10.1093/JPE/RTM005

Xu, H. (2006). Modification of Normalized Difference Water Index (NDWI) to enhance open water features in remotely sensed imagery. *International Journal of Remote Sensing*, 27, 3025–3033. https://doi.org/10.1080/01431160600589179

Yin, J., Gentine, P., Zhou, S., Sullivan, S. C., Wang, R., Zhang, Y., & Gu, S. (2018). The large increase in global storm runoff extremes are driven by climate and anthropogenic changes. *Nature Communications*, 9, 4389. https://doi.org/10.1038/s41467-018-06765-2

Yuan, F., & Bauer, M. E. (2007). Comparison of impervious surface area and normalized vegetation difference index as indicators of surface urban heat islands effects Landsat imagery. *Remote Sensing of Environment*, 106, 375–386.

Zhang, F., Tiyip, T., Kung, H., & Johnson, V. C. (2016). Dynamics of land surface temperature (LST) in response to land use land cover (LULC) change in the Weigan and Kuqa river Oasis, Xinjiang, China. *Arabian Journal of Geosciences*, 9(7), 1-14. https://doi.org/10.1007/s12517-016-2521-8

Zhang, Z., & He, G. (2013). Generation of land SAT surface temperature product for China, 2000–2010. *International Journal of Remote Sensing*, 34, 7369–7375.

Zhang, Z., He, G., & Wang, X. (2010). A practical DOS model-based atmospheric correction algorithm. *International Journal of Remote Sensing*, 31, 2837–2852. https://doi.org/10.1080/01431160903124682

Zhao, H. M., & Chen, X. L. (2005, July 25–29). *Use of normalized difference Bareness Index in quickly mapping bare areas from TM/ETM+* [Conference session]. International Geoscience and Remote Sensing Symposium, Seoul, Vol. 3, pp. 1666–1668.

Zhao, W., He, J., Wu, Y., Xiong, D., Wen, F., & Li, A. (2019). Analysis of land surface temperature trends in the central Himalayan region based on MODIS products. *Remote Sensing*, 11, 900.

Zhou, X., & Wang, Y. C. (2011). Dynamics of land surface temperature in response to land-use/cover change. *Geographical Research*, 49(1), 23–36. https://doi.org/10.1111/j.1745-5871.2010.00686.x